# Hall Effect and Magnetoresistance in Pure Iron, Lead, Fe-Co, and Fe-Cr Dilute Alloys*

A. K. Majumdar[†] and L. Berger

*Physics Department, Carnegie-Mellon University, Pittsburgh, Pennsylvania 15213*
(Received 3 August 1972)

Hall effect and transverse and longitudinal magnetoresistances have been measured in polycrystals at 4.2 K and below, in the fields up to 7 T. For pure iron ($\rho_{300}/\rho_{4.2} = 523$ and 1993), extrapolation of the Hall angle $\phi_H$ to the high-field limit gives a nonzero value $\tan\phi_H = (-2.2\pm0.5)\times10^{-2}$ in agreement with our theory of asymmetric scattering in compensated metals. A nonzero high field, $\tan\phi_H = 2\times10^{-2}$, is also found for pure lead ($\rho_{300}/\rho_{1.5} = 24\,300$) at 1.5 K; this and the nonlinear variation of the Hall resistivity might come from asymmetric scattering by traces of iron impurities known to be present. The Hall-resistivity data for pure iron, dilute Fe-Co, and the iron whiskers of Dheer fall roughly on the same Kohler curve which does not go through the origin. Extrapolation to the low-field limit for Fe-Co gives a nonzero value, $\tan\phi_H = (1.4\pm0.2)\times10^{-2}$, in agreement with asymmetric scattering theory. Kohler's rule holds very well for the transverse magnetoresistance and the Hall resistivity of the Fe-Co alone. It fails completely for the Hall resistivity of Fe-Cr, which seems dominated by the nonclassical "side-jump" mechanism and not by asymmetric scattering. The value of the side-jump $\Delta y$ for Cr impurities in iron at 4 K is eight times as large as the usual value for scatterers in iron at 300 K.

## I. INTRODUCTION

The Hall resistivity in a ferromagnetic polycrystal is usually given[1] by (in mks units)

$$\rho_H = E_y/j_x = R_o B_z + R_s M_z , \qquad (1)$$

where $\vec{j} \parallel \hat{x}$ is the electric current density, $\vec{E}$ the electric field, and $\vec{B} \parallel \hat{z}$ the magnetic induction. The first term has its origin in the Lorentz force acting on the electrons and is present in nonmagnetic materials too. $R_o$ is called the "ordinary" Hall constant. The second term, characteristic of a ferromagnet, depends on the magnetization $\vec{M}$ while $R_s$ is known as the "extraordinary" or the "spontaneous" Hall constant. Two different mechanisms are responsible for $R_s$, namely, the classical Smit asymmetric scattering[2] and the nonclassical transport (side jump).[3]

Many of the existing experimental investigations of the Hall effect in ferromagnets suffer from the following defects: (a) The electron relaxation time is too short for the classical Boltzmann equation to hold.[4,5] The nonclassical "side-jump" mechanism is dominant. (b) The temperature range is such that it is uncertain whether electrons are scattered by magnons, phonons, impurities, or other electrons. In alloys, impure base materials give additional uncertainties on the nature of scatterers. (c) In alloys, the solute concentration is so large that the impurity wave functions are likely to overlap.

Most of these objections are removed if we work at 4 K with pure metals and sufficiently dilute alloys (concentration smaller than 1 at.%) made from zone-refined materials. This experimental situation ensures that the electrons are mostly scattered by isolated and well-defined impurities. Then the dominant mechanism responsible for the spontaneous Hall effect of magnetic materials is often the classical Smit asymmetric scattering of electrons by impurities. This has already been detected in the case of nickel-based alloys.[6,7]

We have detected asymmetric scattering through measurements of Hall effect and magnetoresistance in pure iron, pure lead, and iron-cobalt, as a function of magnetic fields up to 7 T for pure iron and 6 T for the others. The temperature of the experiments is 4.2 K in most cases but some measurements are taken at lower temperatures down to 1.35 K. We find the side-jump mechanism to dominate in the case of dilute iron-chromium alloys under the same conditions.

## II. ASYMMETRIC SCATTERING

We discuss the "asymmetric scattering" of magnetized conduction electrons on impurities, proposed by Smit.[2] In the presence of a spin-orbit interaction there is a left-right asymmetry in the differential scattering cross section. As a result the electrons tend to pile up on one side of the sample producing a transverse electric field.

The parameter $\omega_c\tau$, where $\omega_c$ is the cyclotron frequency and $\tau$ the electron relaxation time, may become large in pure metals or dilute alloys at low temperature. A theory of asymmetric scattering for arbitrary $\omega_c\tau$ was recently developed by Berger,[8] using a two-band model with $n_e$ and $n_h$ number of electrons and holes per unit volume. General expressions were obtained for the tangent of the Hall angle $\tan\phi_H = E_y/E_x$, the transverse

magnetoresistivity $\rho = E_x/j_x$, and the Hall resistivity $\rho_H = E_y/j_x$. They show that, for a given impurity type and constant magnetization $M_g$, Kohler's rules[9] are valid even in the presence of asymmetric scattering, i.e., $\tan\phi_H$, $\rho/\rho_0$, and $\rho_H/\rho_0$ are functions of $B/\rho_0$ alone, where $\rho_0$ is the residual resistivity when $B = 0$. This theory may be easily extended to an arbitrary number of spherical bands of electrons and holes.

In the low-field limit $\omega_c\tau \ll 1$, the above theory gives

$$\tan\phi_H = -\frac{\sigma_e(S^e_{xy}/S^e_{xx}) + \sigma_h(S^h_{xy}/S^h_{xx})}{\sigma_e + \sigma_h} \propto M_g \quad , \tag{2}$$

$$\rho = (\sigma_e + \sigma_h)^{-1} \propto c \quad , \tag{3}$$

$$\rho_H = R_o B_g + R_s M_g \quad , \tag{4}$$

where

$$R_o = \frac{\sigma_e^2/n_e e_e + \sigma_h^2/n_h e_h}{(\sigma_e + \sigma_h)^2} \propto c^o \tag{5}$$

and

$$R_s = -\frac{\sigma_e^2 S^e_{xy}/n_e e_e + \sigma_h^2 S^h_{xy}/n_h e_h}{M_s(\sigma_e + \sigma_h)^2} \propto c \quad . \tag{6}$$

Here the tensors $\vec{S}^e$ and $\vec{S}^h$ have the dimension of the inverse of a mobility. The off-diagonal elements $S^e_{xy}$ and $S^h_{xy}$ describe the asymmetric scattering and are proportional to $M_g$, whereas the diagonal elements $S^e_{xx}$ and $S^h_{xx}$ give the Ohmic resistivity just as in a nonmagnetic metal. All elements of $\vec{S}^e$ and $\vec{S}^h$ are proportional to the impurity concentration $c$. The conductivities are given by $\sigma_e = n_e e_e/S^e_{xx}$ and $\sigma_h = n_h e_h/S^h_{xx}$, where $e_e = -e_h < 0$. Equation (2) shows that there is a nonzero asymptotic value of $\tan\phi_H$ in the low-field limit, caused by asymmetric scattering. In the case of a compensated metal ($n_e e_e + n_h e_h = 0$) such as iron, Eq. (5) gives

$$R_o = \frac{1}{n_e e_e}\left(\frac{\sigma_e - \sigma_h}{\sigma_e + \sigma_h}\right) = \frac{1}{n_e e_e}\left(\frac{1-b}{1+b}\right) \quad , \tag{7}$$

where $b = \sigma_h/\sigma_e$ is the ratio of conductivities of holes and electrons. The sign of $R_o$ determines the relative conductivities of the electron and the hole bands. This is exactly what is obtained in a two-band model without the asymmetric scattering. Combining Eqs. (3) and (6) we get

$$R_s = a\rho \quad , \tag{8}$$

where $a = \tan\phi_H/M_s$ is a constant of proportionality. In the high-field limit we get for a compensated metal ($n_e e_e + n_h e_h = 0$) such as iron,

$$\tan\phi_H = \frac{\sigma_e^{-1}(S^e_{xy}/S^e_{xx}) + \sigma_h^{-1}(S^h_{xy}/S^h_{xx})}{\sigma_e^{-1} + \sigma_h^{-1}} \propto M_g \quad , \tag{9}$$

$$\rho \propto B_g^2/c \quad , \tag{10}$$

$$\rho_H \propto M_g B_g^2/c \quad . \tag{11}$$

Equation (9) implies a nonzero asymptotic value of $\tan\phi_H$ in the high-field limit, caused by asymmetric scattering. It is to be noted from Eqs. (2) and (9) that, in the special cases when $\sigma_e = \sigma_h$ or when $S^e_{xy}/S^e_{xx} = S^h_{xy}/S^h_{xx}$, the low- and the high-field asymptotic values are equal in magnitude and opposite in sign. The magnetoresistance as given by Eq. (10) is the usual one for a compensated metal. The $M_g B_g^2/c$ term in Eq. (11) is observable only in case of a very pure metal.

It should be emphasized here that the usual two-band model[1] without asymmetric scattering predicts that $\tan\phi_H$ should vanish in both the low- and high-field limits for a compensated metal.

Previous measurements of Hall effect in iron by Volkenshtein and Fedorov[10] and Dheer[11] are not suitable for high-field extrapolation as $\omega_c\tau$ was rather small.

Reed and Fawcett[12] concluded from high-field magnetoresistance measurements on iron single crystals that it is a compensated metal with some open orbits. Since our iron samples are polycrystalline rods, for some orientations of the grains the magnetic field will give rise to open orbits. This high-field effect is not taken into account in the usual two-band model.[1] The more general theory without asymmetric scattering, developed by Lifshitz, Azbel, and Kaganov, is discussed by Fawcett.[13] It is shown that although the open orbits may affect $\rho_H$ and $\rho$, $\tan\phi_H$ would still vanish as $1/B$ except in a "singular field direction," which is presumably a zero-probability event in a polycrystal in the high-field limit.

## III. ORDER OF MAGNITUDE OF ASYMMETRIC SCATTERING IN THE LOW-FIELD LIMIT

First we summarize the results obtained by Smit[2] for the scattering of free electrons by a square-well impurity potential $V(r)$ in the presence of the spin-orbit interaction. If $R$ is the range of the potential,

$$V = (\hbar^2/2m)(k^2 - k_1^2) \quad , \quad r < R$$
$$V = 0 \quad , \qquad\qquad r > R \tag{12}$$

where $k$ and $k_1$ are the wave numbers of the electron outside and inside the well, respectively. The solutions of the Schrödinger's equation for the above potential in spherical coordinates are[2,3(a)]

$$\psi^v = \sum_{l=0}^{\infty} a_l j_l(k_1 r) P_l(\cos\theta) \quad , \qquad r < R$$
$$\psi^v = e^{i\vec{k}\cdot\vec{r}} + \sum_{l=0}^{\infty} b_l h_l(kr) P_l(\cos\theta) \quad , \quad r > R \quad . \tag{13}$$

The wave vector $\vec{k}$ is chosen along the polar axis $\hat{x}$ and the electron spin along the $\hat{z}$ axis (the angle $\phi$ being measured from $\hat{z}$ axis). The spin-orbit Hamiltonian $H_{so}$, given by

$$H_{so} = \left(\frac{1}{2m^2c^2}\right)\left(\frac{1}{r}\right)\left(\frac{\partial V}{\partial r}\right)S_z L_z \ , \tag{14}$$

is added. The wave function becomes $\psi = \psi^v + \psi^{so}$, with

$$\psi^{so} = \sum_{l=0}^{\infty} p_l j_l(k_1 r) \sin\phi \ \frac{d}{d\theta} P_l(\cos\theta) \ , \quad r < R$$

$$\psi^{so} = \sum_{l=0}^{\infty} q_l h_l(kr) \sin\phi \ \frac{d}{d\theta} P_l(\cos\theta) \ , \quad r > R \ . \tag{15}$$

We keep only $s$- and $p$-wave phase shifts on the assumption of a short-ranged potential. Then the total scattering cross section, or the reciprocal $S_{xx}$ of the mobility, obeys

$$S_{xx} \propto \left| b_0 \right|^2 \tag{16}$$

if the $s$-wave phase shift is much larger than the $p$-wave phase shift. The tangent of the Hall angle is

$$\tan\phi_H = -S_{xy}/S_{xx} = -2\text{Im}(q_1 b_0^*)/3\left| b_0 \right|^2 \ . \tag{17}$$

We have calculated $b_0$ and $q_1$ from the boundary conditions at $r = R$, keeping only the $s$ and $p$ waves, and assuming $k$ and $k_1$ to be real-valued:

$$b_0 = \frac{(\sin\beta \cos\alpha/\beta) - (\sin\alpha \cos\beta/\alpha)}{(i \cos\alpha/\beta) + (\sin\alpha/\alpha)} e^{-i\beta} \ , \tag{18}$$

$$q_1 = -i\left(\frac{\hbar}{2mcR}\right)^2 (\alpha^2 - \beta^2)\left(\frac{3}{\beta}\right)e^{-2i\beta}(3\times10^4)$$

$$\times \left[\frac{(-\cos\alpha/\alpha) + (\sin\alpha/\alpha^2)}{(-i\cos\alpha/\alpha) + (i\sin\alpha/\alpha^2) - \sin\alpha(i/\beta^2 + 1/\beta)}\right]^2 \ , \tag{19}$$

where
$$\alpha = k_1 R, \quad \beta = kR,$$
and
$$V = \frac{\hbar^2}{2mR^2}(\beta^2 - \alpha^2) \ .$$

In Eq. (14) we have considered only the spin-orbit interaction associated with the impurity potential. As shown by several authors,[2,14] the combined effect of the impurity potential and of a periodic lattice potential is to yield an effective spin-orbit Hamiltonian which is similar in form to Eq. (14), but with a coupling parameter enhanced by a factor of $\approx 3\times10^4$. This enhancement factor has been included in Eq. (19).

In the case of very repulsive impurity potential $V$, $k_1$ and $\alpha$ become imaginary [see Eq. (12)]. It is convenient to introduce the quantity $\alpha' = i\alpha$ in that range in order to work with real quantities. The potential will still be proportional to $\beta^2 - \alpha^2 = \beta^2 + (\alpha')^2$ but $\alpha^2$ will take negative values. Then the coefficients $b_0$ and $q_1$ are given by

$$b_0 = \frac{(\sin\beta \cosh\alpha'/\beta) - (\sinh\alpha' \cos\beta/\alpha')}{(i \cosh\alpha'/\beta) + (\sinh\alpha'/\alpha')} e^{-i\beta} \ , \tag{20}$$

$$q_1 = -i\left(\frac{\hbar}{2mcR}\right)^2 [\beta^2 + (\alpha')^2]\left(\frac{3}{\beta}\right)e^{-2i\beta}(3\times10^4)\left[\frac{(-\cosh\alpha'/\alpha') + [\sinh\alpha'/(\alpha')^2]}{(\cosh\alpha'/\alpha') - [\sinh\alpha'/(\alpha')^2] + \sinh\alpha'(-1/\beta^2 + i/\beta)}\right]^2 \ . \tag{21}$$

The range of the potential $R = 0.026$ nm is approximately obtained from the atomic spin-orbit parameter for iron ($\approx 0.1$ eV), and Eq. (14) applied to a Coulomb potential. Taking the electron energy $E \approx 1.7$ eV (a reasonable guess for the Fermi energy of $3d$ electrons in iron) we get $\beta \approx 0.2$ from the relation $E = \hbar^2 k^2/2m = \hbar^2 \beta^2/2mR^2$, assuming free-electron mass. Of course this value is very rough. A simple computer program was written to calculate $S_{xx}$ and $\tan\phi_H = -S_{xy}/S_{xx}$ as a function of $\beta^2 - \alpha^2 = \beta^2 + (\alpha')^2$, using the effective $H_{so}$. These are plotted in Fig. 1 where both $S_{xx}$ and $\tan\phi_H$ show $s$-type resonances for attractive potentials and a saturation effect for large repulsive potentials. The top of the resonances is not shown. These resonances and the very repulsive limit were not studied by Smit.[2] $\tan\phi_H$ is odd with respect to the impurity potential, as Eqs. (17)–(21) would imply, to lowest order in the potential. Also the resonances of $S_{xx}$ and $\tan\phi_H$ are approximately $\pi/2$ apart in $\alpha$. In the limit of infinite repulsive potential ($\alpha \to \infty$) and small po-

tential range ($\beta \to 0$), Eqs. (17), (20), and (21) give

$$\tan\phi_H \approx -(3\times10^4)\times 2(\hbar/2mcR)^2\beta^3 \ . \tag{22}$$

For $\beta = 0.2$ we obtain $\tan\phi_H \approx -2\times10^{-2}$ in agreement with the extreme right side of Fig. 1.

On Fig. 1, $\tan\phi_H$ is positive almost everywhere in the region to the left of the origin. However, if we were to choose a larger value of $\beta$, the complex argument of $q_1$ would become sizably different from $\pi/2$, and $\tan\phi_H$ would be negative in a larger region close to each antiresonance. This is indicated roughly by a dotten line in Fig. 1.

Huguenin and Rivier[6] studied experimentally asymmetric scattering in dilute nickel alloys and found in the low-field limit $\tan\phi_H \approx -1.1\times10^{-2}$ for Ni-Fe and Ni-Co and $\approx -2.2\times10^{-2}$ for Ni-Cu alloys. One way of explaining the same sign of $\tan\phi_H$ in Ni alloys for different signs of the impurity potential is to assume that, for minority spin carriers in Ni-Fe and Ni-Co, we are on the dotted line at the left of point $C$ (Fig. 1), while in Ni-Cu
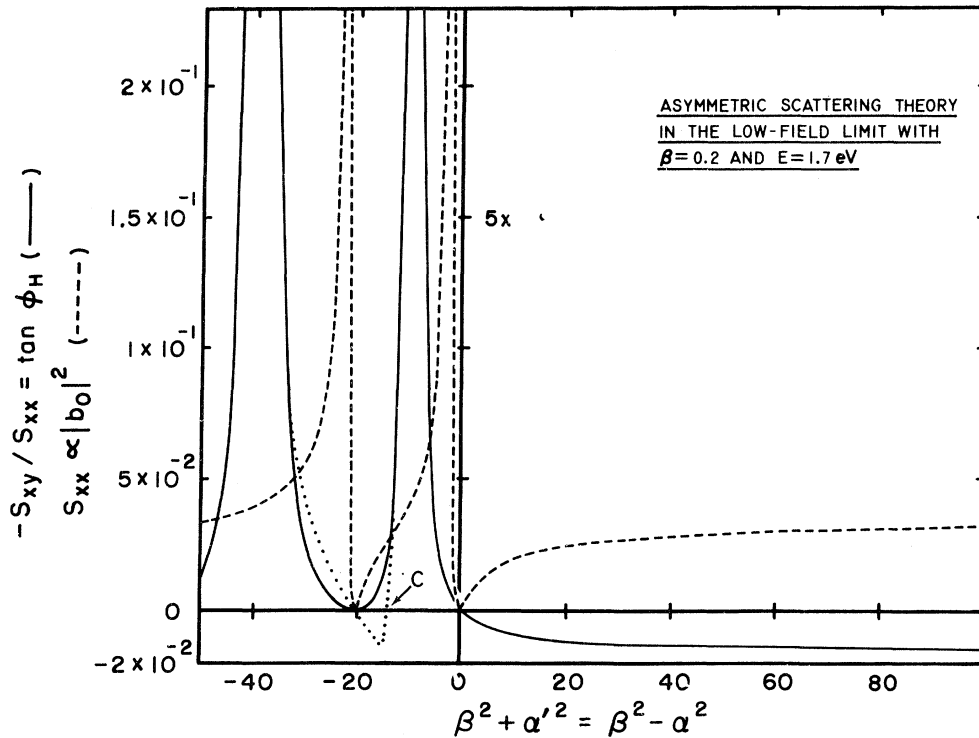
FIG. 1. Ohmic resistivity $(\propto S_{xx})$ and the tangent of the Hall angle, $\tan\phi_H$, as a function of impurity potential $(\propto \beta^2 - \alpha^2)$ according to asymmetric scattering theory in the low-field limit. All curves are for $\beta = 0.2$ except the dotted line which shows roughly the effect of a larger value of $\beta$. Point $C$ shows an additional change of sign of $\tan\phi_H$ for the latter case. The $S_{xx}$ curve does not have any cusp at the origin.

we are on the right side of the origin.

The main defect of the present theory is that it treats $s$-wave resonances instead of the $d$-wave resonances really found in Ni and Fe. Fert and Jaoul[7] have recently published a very interesting study of $d$-wave resonances, which seems to predict a change of sign of $\tan\phi_H$ sometime after the resonance has passed through the Fermi level (similar to the dotted line on Fig. 1).

The residual resistance of dilute ferromagnetic Ni alloys with transition-element impurities at 4.2 K has been measured by Chen.[15] He found that the residual resistivity shows a very sharp resonance when chromium is dissolved; the resistivity is very small for elements between Cu and Mn, and then there is an abrupt jump from Mn to Cr and a rapid decrease upon continuing to V and Ti. This behavior can also be explained[16] in terms of the effect of scattering resonances on the inverse mobility $S_{xx}$ (Fig. 1). Recently Arajs $et$ $al.$[17] found a similar resonance in dilute iron alloys at 4.2 K when the solute atom is chromium, but the resonance is not so sharp as in Ni alloys.

It is interesting to see whether the resonance in the Fe-Cr electrical resistance is also found experimentally for $\tan\phi_H$, and whether the two reso-

nances are shifted with respect to each other as predicted by our square-well model.

## IV. NONCLASSICAL TRANSPORT

It has been shown[4,5] that, if the dimensionless parameter $\hbar/\tau E_F$ becomes large, where $\tau$ is the electron relaxation time and $E_F$ is the Fermi energy, the classical Boltzmann equation does not hold and nonclassical terms begin to dominate. This corresponds to the cases of concentrated alloys or high temperatures. Luttinger[5] calculated the Hall effect of ferromagnets on the basis of quantum transport theory, and found a term $R_s = A\rho^2$, not predicted by classical asymmetric scattering, which leads rather to $R_s = a\rho$ [Eq. (8)].

Recently Berger[3(a)] has suggested an intuitive picture for the Hall effect of ferromagnets above 100 K which, in a sense, gives the physical interpretation of the mathematical model developed by Luttinger. He has proposed that, owing to the spin-orbit interaction in a ferromagnet, an electron undergoes a discontinuous and finite "side jump" at every scattering by impurities or phonons. This also leads to the equation

$$R_s = A\rho^2 \ . \tag{23}$$

With the assumptions of Born approximation and short-range potential it is shown that the constant of proportionality $A$ is the same for scattering by different impurities. It is also suggested that the phonon scattering might give the same constant. The side jump $\Delta y$ can be expressed (for a one-band model) in terms of $A$ as

$$\Delta y = AM_s \hbar k_F / ne^2 \ , \tag{24}$$

where $M_s$ is the saturation magnetization, $k_F$ the Fermi wave number of the electron, and $n$ the number of electrons per unit volume.

Lyo and Holstein[3(a)] have shown that $\Delta y$ is completely independent of potential range and shape, if the $3 \times 10^4$ spin-orbit enhancement factor is assumed constant, in the Born approximation.

Jellinghaus and De Andres[18] found for several dilute iron alloys at room temperature, containing Si, Ti, V, Cr, Mn, Co, Ni, and Cu impurities, that $R_s = (4 \times 10^4) \rho^{2.08}$ over almost two decades of resistivity, where $R_s$ is in (m³/C) and $\rho$ is in ($\Omega$ m). Kooi,[19] Jan,[20] and Jan and Gijsman[21] observed that $R_s = (6 \times 10^4) \rho^{1.9}$ in pure iron and dilute Fe-Si over a wide range of temperatures. Substituting $M_s = 2.18$ T, the rough values $k \approx 10^{10}$ m⁻¹, $n \approx 5 \times 10^{28}$ electrons/m³, and $A$ from the above high-temperature data, we get from Eq. (24) $\Delta y \simeq 0.1$ nm. The neutron scattering experiments[22] show that the magnetic moment disturbance of the above impurities in iron are all localized. Thus the assumption of a short-ranged potential in obtaining Eq. (24) is well justified. The above experimental facts agree quite well with the predictions of the side-jump theory.

Kohler's rule (Sec. II) fails in the case of the side-jump mechanism and is replaced by[3(a)]

$$\rho_H / \rho_0 = f(M_z \Delta y / \Lambda, B_z / \rho_0) \ , \tag{25}$$

where $\Lambda$ is the electron mean free path.

To first order in $\Delta y / \Lambda$, and since $1/\Lambda \propto \rho_0$, this may be written

$$\rho_H / \rho_0 = f_0(B_z / \rho_0) + M_z \rho_0 f_1(B_z / \rho_0) \ , \tag{26}$$

where $f_0$ is an odd function, and $f_1$ an even function. The second term represents the effect of the side jump, while the first term is the ordinary Hall effect.

### V. ANTIFERROMAGNETIC CHROMIUM IMPURITY IN IRON

The neutron elastic scattering data[23] show that the chromium spin is antiferromagnetically aligned in iron. Izyumov and Medvedev[24] developed the theory of an impurity atom in a ferromagnetic crystal, having an antiferromagnetic exchange interaction with the matrix. They predicted the existence of virtually bound spin-wave modes, analogous to electronic virtually bound states. Even when the temperature is so low that these spin-

wave modes are not excited, the sizable zero-point motion of oppositely oriented spins causes a reduction of the projection of the spin of the impurity atom along the spontaneous magnetization. This is compensated by a contraction of the spins of the matrix. This contraction is propagated in the matrix and goes as $e^{-2\alpha x}$, where $x$ is the distance measured from the impurity atom and

$$\alpha = \frac{1}{a} \left( \frac{|E_s|}{2JSz} \right)^{1/2} \ . \tag{27}$$

Here $a$ is the lattice spacing, $S$ the spin of the matrix, $z$ the number of nearest neighbors, and $E_s$ is the energy of the $s$-type virtually bound spin-wave mode.

Equation (27) shows that, the smaller the energy of the mode, the further the zero-point disturbance (here the spin contraction) propagates in the matrix. Kroó et al.[25] showed the existence of an $s$-type virtual spin-wave state in dilute Fe-Cr alloys from neutron inelastic scattering experiments. The mode energy is only $E_s \simeq 1.2$ meV, at low temperature. If we substitute the values of $a$, $J$, $S$, $z$ for iron and the above value of $E_s$ in Eq. (27), we obtain a range, $1/2\alpha \simeq 1.8$ nm.

Direct evidence of the correlation between range of the spin disturbance and energy of the spin-wave mode actually exists in the inelastic neutron scattering data[25] for Fe-Mn, Fe-Cr, and Fe-Er.

Such long-range zero-point spin disturbance might cause considerable small-angle scattering of electrons. This is not expected to affect the electrical resistivity, and indeed our recent resistivity measurements[26] in the range around $T \approx E_s / k_B \approx 14$ K, where the long-range localized magnon mode should become excited, fail to show any spin-disorder resistivity. But it may affect the Hall data. This will be discussed in Sec. X.

The Cr electronic bound state may also cause a long-range disturbance.[16]

### VI. SAMPLES AND THEIR THERMAL TREATMENTS

The pure-iron sample I and the Fe-Co and Fe-Cr dilute alloys were obtained from Materials Research Corp. (MRC). Using three-pass electron-beam zone-refined iron, the alloys were arc melted by MRC in an inert atmosphere of high-purity argon. Then they were cold swaged and cut to size. The pure-iron sample I' was kindly given to us by Schwerer of the U. S. Steel Corp. Research Center. All the samples are cylindrical rods of diameter $\approx 3.1$ mm and length $\approx 25$ mm. The alloys were etched with aqua regia. Then the Fe-Co alloys were annealed in a wet-$H_2$ atmosphere, obtained by bubbling ultrahigh-purity hydrogen through previously degassed distilled water, at a temperature of 1300 °C for a period of 24 h. Wet hydrogen is essential for the removal of impurities

such as carbon and nitrogen in iron.[27,28] To remove the hydrogen from the samples, we annealed them in a vacuum ($p = 3 \times 10^{-5}$ torr) for $2\frac{1}{2}$ h at 850 °C. The samples were then furnace cooled The Fe-Cr alloys were treated in the same way except that they were annealed in a dry-hydrogen atmosphere, since chromium is more oxidizable than the impurities that we were trying to remove. Instead of a bubbler, a liquid-nitrogen trap was set up. The temperature of vacuum annealing (850 °C) was chosen to be below the $\alpha$-$\gamma$ phase transition temperature ($\approx 900$ °C) for both Fe-Co and Fe-Cr.

The pure-iron samples were not treated thermally, to avoid contamination.

The main impurities, i.e., cobalt and chromium, were very accurately determined by Ledoux and Co., using atomic absorption and colorimetric methods (Table I). Analyses of different pieces of the same alloy show that the main impurity concentration differs by at most 0.02 wt% from one piece to the other, indicating that the samples are macroscopically homogeneous. The alloys were spectrographically analyzed for all metallic impurities by Spectrochemical Laboratories in Pittsburgh. Traces of Si, Mo, Ni, Mn, V, and Sn were found. Residual resistance data (Table I) give a more reliable estimate of sample purity, which includes metalloids not visible by spectrography.

The lead is 99.999%-pure material (ASARCO grade A-58). It was machined to a rod of length $\simeq 2.32$ cm and diameter $\simeq 0.3$ cm. The sample was etched in a solution of hydrogen peroxide and acetic acid (1:2), and annealed in a vacuum ($p = 2 \times 10^{-6}$ torr) for 43 h, at 277 °C to remove strains. It was then furnace cooled. The spectrographic analysis supplied by the manufacturer shows that Si, Cu, Mg, and Fe are present, in amounts equal to or smaller than one part per million in weight each.

### VII. SAMPLE HOLDER AND MEASURING CIRCUIT

Two fixed Micarta clamps encircle the sample close to its ends, and hold it in a given orientation. Each clamp, which may be tightened by screws, also serves to press an iron wire against the side of the sample. These wires are the potential probes used in measurements of the Ohmic resistance.

A third clamp encircles the middle of the sample and presses two wires tangentially against opposite sides of the sample. These wires, made of the same material as the sample, are used as Hall probes. The Hall clamp rides freely on the sample, and follows it if it happens to move slightly under magnetic forces. The Hall wires must be positioned as accurately as possible in the same plane normal to the sample axis, in order to minimize the contribution of Ohmic voltages. The Hall and resistance wires were annealed at the same time as the corresponding samples. They go to two small copper boxes, where they are soldered to No. 24 copper wires which run to the top of the Dewar vessel. Sample and copper boxes are directly immersed in liquid helium.

The magnetic field is provided by a 38-mm-bore Nb-Ti superconducting magnet. After Hall effect

TABLE I. Summary of sample properties. $R_o$ refers to the low-field limit for the alloys, high-field limit for pure metals. $R_s$ always refers to the low-field limit, and $r$ to an intermediate-field range [Eq. (28)]. The temperature is 4.2 K, unless specifically mentioned otherwise.

| Sample No. | Solute concentration | $\rho(B_{ext}=0)$ $(10^{-10}\ \Omega\ m)$ | $\rho_0 = \rho(B=0)$ $(10^{-10}\ \Omega\ m)$ | Residual resistivity ratio $(\rho_{300}/\rho_0)$ | $R_o$ $(10^{-11}\ m^3/C)$ | $R_s$ $(10^{-11}\ m^3/C)$ | $r$ $(10^{-11}\ \Omega\ m)$ |
|---|---|---|---|---|---|---|---|
| I | Pure iron | 4.357 | 1.910 | 523 | $-7.6$ | $\cdots$ | 4.4 |
| I′ | Pure iron | $4.12 \pm 0.56$ | 0.502 | 1993 | $-12.2$ | $\cdots$ | 5.7 |
| Fe7 of Dheer (Ref. 11) | Pure-iron single crystal | 2.183 | 1.158 | 863 | $-9.6$ | $\cdots$ | 3.05 |
| L | Pure lead | 0.082 at 1.5 K | 0.082 at 1.5 K | 24 300 at 1.5 K | 17 at 1.5 K and 0.4 $T$ | $\cdots$ | $\cdots$ |
| II | 0.25 wt% Co | 26.6 | 22.9 | 45.2 | $-1.75$ | 1.51 | $\cdots$ |
| III | 0.50 wt% Co | 46 | 42.9 | 25.2 | $-1.35$ | 2.70 | $\cdots$ |
| V | 0.92 wt% Co | 94 | 91 | 12.5 | $-1.41$ | 6.06 | $\cdots$ |
| 1 | 0.25 wt% Cr | 91 | 85 | 14.0 | 8.32 | 3.85 | $\cdots$ |
| 2 | 0.54 wt% Cr | 166 | 160 | 7.73 | 11.80 | 14.14 | $\cdots$ |
| 3 | 0.98 wt% Cr | 274 | 274 | 5.56 | 12.00 | 37.09 | $\cdots$ |
| 1 of Carter and Pugh (Ref. 47) | 0.70 wt% Cr | 199 | 195 | 7.20 | 17.10 | 26.30 | $\cdots$ |

and transverse magnetoresistance have been mea-
sured with sample axis normal to magnet axis,
the sample is reoriented for the longitudinal mag-
netoresistance measurements.

Hall and resistance voltages are measured by
a Keithley 148 nanovoltmeter, which is a high-
gain, battery-powered, chopper amplifier with a
resolution of $\pm 10^{-9}$ V. The nanovoltmeter output
is fet into a United Systems Corp. 251 A digital
millivoltmeter through a Keithley 399 isolating
amplifier. The nanovoltmeter calibration is
checked with a Rubicon Thermofree potentiometer,
used as a low-impedance voltage source.

Sample current ($\approx 20$ A) and magnet current are
measured by two shunts connected to another
digital millivoltmeter. The outputs from the two
digital millivoltmeters go to a United Systems
Corp. 611E/620E printing system.

Owing to the small value ($\approx 10^{-6}$ V) of the Hall
voltages, precautions such as careful shielding of
circuit,[29] elimination of loop areas in magnetic
field, minimization of thermoelectric voltages, and
battery operation, and floating of nanovoltmeter
are essential. Sample current is reversed after
each data point, and magnetic field is reversed in
the middle of each run, to isolate in the usual
manner[1] the Hall voltage from other voltages.
The Ohmic voltage coming from Hall-probe mis-
alignment may be eliminated by field reversal only
if it is reproducible throughout the run, and is not
too large. This is checked carefully during the
runs.

## VIII. RESULTS FOR PURE IRON AND Fe-Co ALLOYS

Figure 2 shows the longitudinal magnetoresis-
tance of the two pure-iron samples I and I' as a
function of the external magnetic field at 4.2 K.

The negative magnetoresistance in small ex-
ternal fields below saturation (Fig. 2) is often
found in pure iron and nickel at low temperature,
and can be explained[30,31] in terms of the magneto-
resistance caused in each Weiss domain by the
internal field $\vec{B} = \vec{M}_s = 2.2$ T which exists even in
the absence of any external field. The external
field $\vec{B}_{ext}$ merely realigns these internal fields.
It is possible to find a value of $\rho$, called $\rho_0$, which
in principle has no magnetoresistive contributions,
by extrapolating the pure-iron data above satura-
tion back to $B = 0$, as was done by Schindler and
La Roy.[31] Nevertheless, we have chosen the min-
imum value of $\rho$ (at $B_{ext} \approx 0.4$ T) as our $\rho_0$ since
the extrapolation seems to be quite uncertain.[32]
The residual resistance ratios $\rho_{300}/\rho_0$ and the
values of $\rho_0$ are tabulated in Table I. The resis-
tivity at $B_{ext} = 0$ for sample I' varies considerably
from one run to the other. This results from the
lack of reproducibility of the demagnetized state.
The magnetoresistance data of sample I' in a
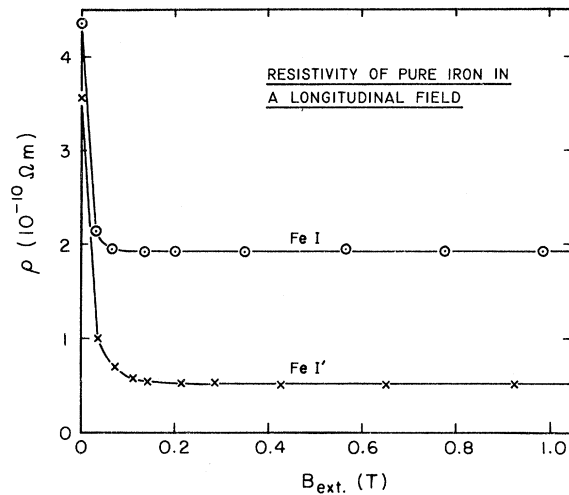


FIG. 2. The longitudinal magnetoresistance $\rho$ of pure
iron is plotted vs the external magnetic field at 4.2 K.

longitudinal field of 0.4 T between 4.2 and 1.46 K,
on extrapolation to 0 K, show that 11% of the re-
sistivity at 4.2 K is contributed by electron-elec-
tron scattering, phonons, or other causes of ther-
mal scattering. This contribution is obviously
much smaller for the less-pure sample I and all
the dilute alloys. Thus in our experiments the
electrons are mostly scattered by impurities.

In the case of Fe-Co alloys, the longitudinal
magnetoresistance data above saturation are ex-
trapolated to $B = 0$ to obtain an approximate $\rho_0$
(samples II, III, and V). However, the $\rho_0$ values
are then slightly adjusted (as a matter of fact
only sample III has to be adjusted by 2%) in such
a way that the Kohler's rule for longitudinal mag-
netoresistance holds for the three alloys put
together. These adjusted values of $\rho_0$ are tab-
ulated in Table I together with the resistivity
ratios. Figure 3 shows the Kohler plot for longi-
tudinal magnetoresistance where we have plotted
$\rho/\rho_0$ against $B/\rho_0$ for all three samples. This
procedure was followed by Schwerer and Silcox[33]
in the case of nickel alloys. In our case, the
validity of Kohler's rule for the transverse mag-
netoresistance, with the same choice of $\rho_0$, will
check the correctness of the above procedure.
The choice of $\rho_0$ is quite critical because the mag-
netoresistances are quite small for these alloys.
We show only data above saturation. For longi-
tudinal fields, we have in the rod $B \approx B_{ext} + M_s$,
where $M_s \approx 2.18$ T.

The residual resistivity $\rho_0$ when plotted as a
function of cobalt percentage gives an approximate
straight line [see Eq. (3)] with a slope of
$9.2 \times 10^{-9}$ $\Omega$ m/wt% and a very small intercept.
The latter clearly shows that the concentration of
all other impurities put together is much smaller
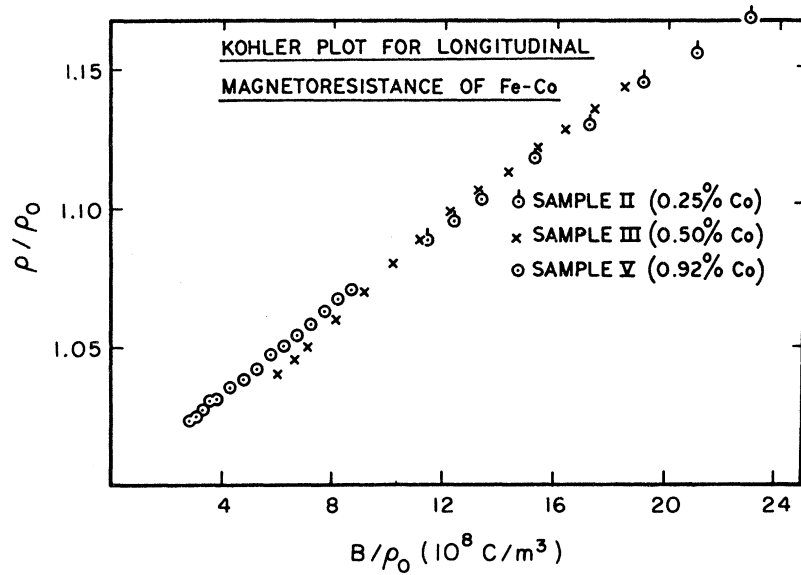
FIG. 3. Kohler plot for the longitudinal magnetoresistance $\rho$ of Fe-Co dilute alloys at 4.2 K.

than that of cobalt. Moreover, our measured slope agrees very well with the average value of $9.4 \times 10^{-9}$ $\Omega\,m/wt\%$ of the slopes obtained by Arajs *et al.*[17] and by Schwerer and Cuddy[34] for Fe-Co alloys at 4.2 K.

Figure 4 shows the Kohler plot for transverse magnetoresistance above saturation of the pure-iron samples I and I′ and the dots represent the Fe-Co alloys. Here we use $B = B_{ext} + M_s/2$. The behavior in $B^2$ is typical of a compensated metal

[see Eq. (10)].

We have plotted the transverse magnetoresistance of the three dilute alloys alone on a Kohler plot in Fig. 5. Kohler's rule is satisfied extremely well here. This shows that our choice of $\rho_0$ from longitudinal magnetoresistance data is meaningful.

We have plotted in Fig. 6 the Hall resistivity data for the pure-iron samples I and I′, together with those of Dheer[11] for iron whiskers, on a
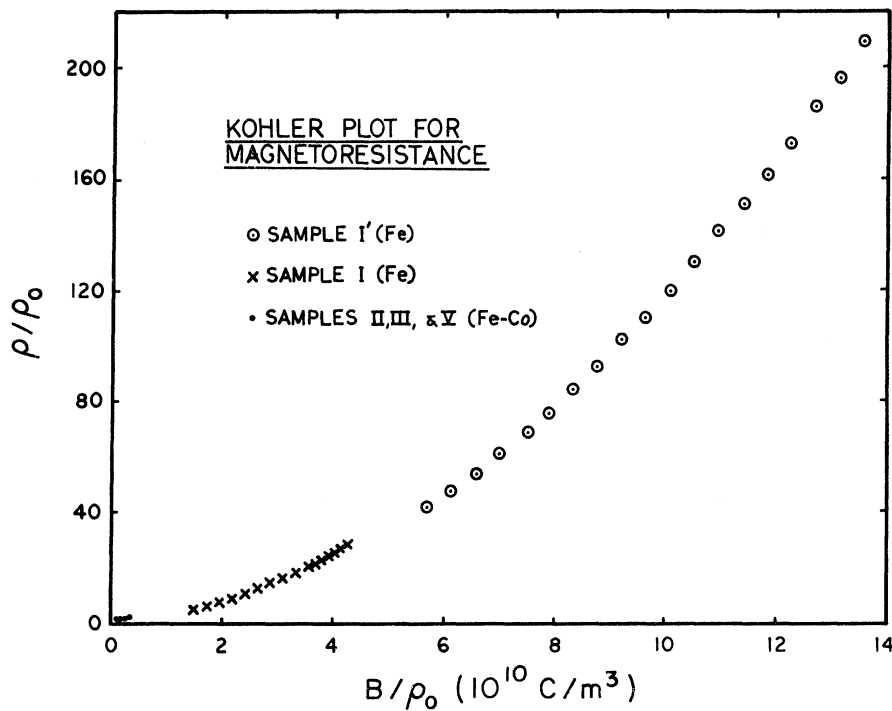


FIG. 4. Kohler plot for the transverse magnetoresistance $\rho$ of pure iron and Fe-Co dilute alloys at 4.2 K.
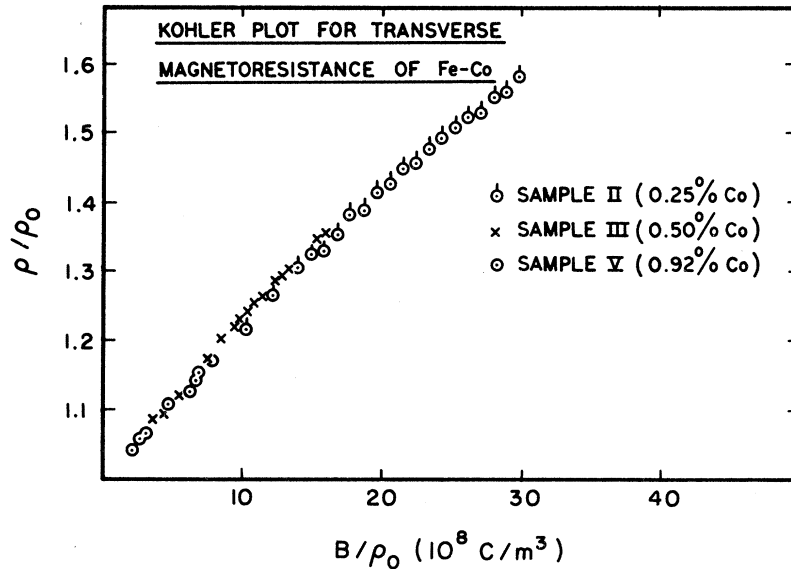
FIG. 5. Kohler plot for the transverse magnetoresistance $\rho$ of Fe-Co dilute alloys at 4.2 K, on an enlarged scale.

Kohler plot. They are located nearly on the same Kohler curve. This is the first time a Kohler plot is drawn for the Hall effect of iron. Now it is possible to interpret the data of different samples of varying purities on a more general basis. The dots near the origin show the data for the Fe-Co alloys (later on magnified).

If we extrapolate the "high-field" pure-iron data linearly back to $B/\rho_0 = 0$, we find a large intercept. By large, we mean that, if we calculate the tangent of the Hall angle at $B/\rho_0 = 0$ from this intercept, we get $\tan\phi_H \approx 0.2-1.2$. This intercept is related to the curvature of the Kohler curve at $\omega_c\tau \approx 1$. It is not associated with ferromagnetism or asymmetric scattering, and can be easily simulated by

three or more bands of different mobilities in any compensated metal. We have used a four-band model. Assuming $S_{xx}^1 = -5.963$ T, $S_{xx}^2 = 3.105$ T, $S_{xx}^3 = -5.964$ T, $S_{xx}^4 = 12.734$ T, $n_1 = n_2 = 0.581$ $\times 10^{28}$ electrons/m$^3$, $n_3 = n_4 = 2.07 \times 10^{28}$ electrons/ m$^3$, $e_1 = -e_2 = e_3 = -e_4 = -1.6 \times 10^{-19}$ C, we obtain the middle curve of Fig. 7. It should be emphasized that this is an intermediate-field behavior; at still higher fields, the Kohler curve would curve back to give a vanishing intercept. This was not stressed enough in Ref. 8.

These large apparent intercepts, and the curvature of Kohler curve, are the real and simple explanation of the "giant" values of the spontaneous Hall coefficient $R_s$, claimed by Fivaz[35] to be present
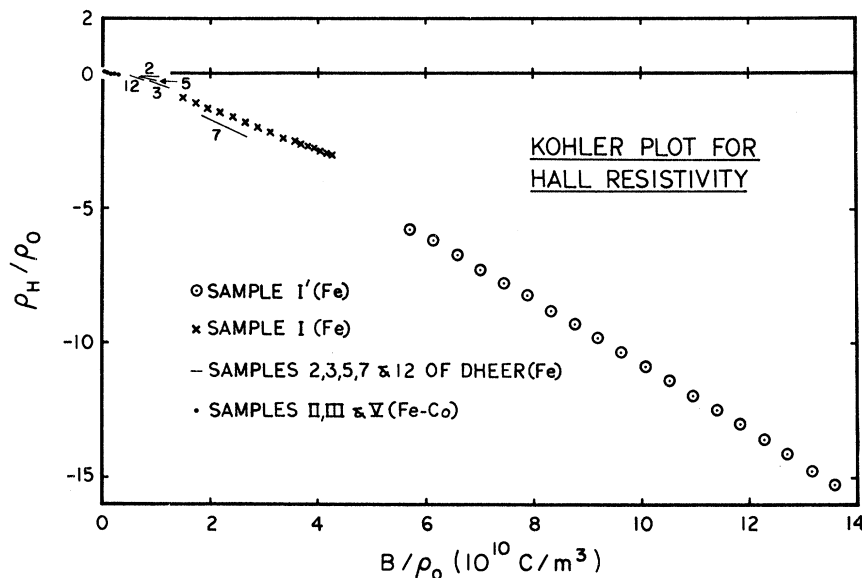


FIG. 6. Kohler plot for the Hall resistivity $\rho_H$ of pure iron and Fe-Co dilute alloys at 4.2 K.

in the Dheer pure-iron data[11] at low temperature and explained by him in terms of an orbital degeneracy of the band structure of iron. These intercepts can be understood best by drawing a Kohler plot. Since they may exist even in nonmagnetic metals,[36] they should not be described by a coefficient $R_s$ [Eq. (1)], but rather by a new coefficient $r$ and the rough relation[8,37]

$$\rho_H \approx R_0 B_z + r \, \text{sgn} B_z \qquad (28)$$

valid at intermediate fields.

The Hall data for our sample I' are not included in Fig. 7 because they correspond to higher $\omega_c \tau$ values, making the intercept determination too uncertain. Actually, the curve for sample I' is slightly concave downwards (Fig. 6). Since this curvature seems to persist up to the highest $\omega_c \tau$ values, it may not be caused by intermediate-field multiband effects but rather by the $M_z B_z^2/c$ associated with asymmetric scattering at $\omega_c \tau \gg 1$. These high-field effects [Eqs. (9)–(11)] are treated in more detail in Sec. IX.

The Kohler plot for the tangent of the Hall angle is shown for the pure-iron samples and the Fe-Co alloys in Fig. 8. From Figs. 4, 6, and 8 it is obvious that Kohler's rules hold only roughly for pure materials, where it is very difficult to identify and control the nature of impurities. In part for the same reason, we think that Ehrlich et al.[38] (Ni) and Wagenblast and Arajs[39,40] (Fe) found a disagreement in the case of pure metals.

The effect of asymmetric scattering on the Kohler curve for the Hall resistivity can be detected by a closer look at the low-field region. The data for the three dilute alloys are magnified

in the Kohler plot for the Hall resistivity in Fig. 9 where the curve does not go through the origin, and Kohler's rule is very well satisfied. Extrapolation to $B/\rho_0 = 0$ gives the low-field asymptotic value $\tan\phi_H = \rho_H/\rho_0 = 1.4 \times 10^{-2}$.

We have discussed in Sec. II the fact that Kohler's rule for the Hall resistivity holds for asymmetric scattering but not for the nonclassical transport. So, in plotting Fig. 9, we have subtracted from our data the nonclassical Kohn–Luttinger contribution (or side-jump contribution). Equation (23) gives $R_s = A\rho^2$, and we have used[18-21] $A = 6 \times 10^4 \, \text{m}/\Omega^2$ as discussed in Sec. IV. Combining this with Eq. (1) and taking $\rho = \rho_0$ the corrections to $\rho_H/\rho_0$ amount to approximately $0.03 \times 10^{-2}$, $0.06 \times 10^{-2}$, and $0.12 \times 10^{-2}$ for the samples II, III, and V, respectively. Obviously, this correction should be negligible for the pure iron. The correction here is assumed to be field independent. It is quite possible that the deviation of the curve for the sample II from those of III and V may be explained in terms of a field-dependent correction. It should be emphasized here that even the largest correction is much smaller than the asymptotic value of $\tan\phi_H$ obtained by low-field extrapolation. This implies that we know the asymptotic value with a fairly good accuracy and so we take it as $\tan\phi_H = (1.4 \pm 0.2) \times 10^{-2}$. This is the same order of magnitude mentioned in Sec. III for Ni alloys.

The Hall constants $R_0$, $R_s$ [Eq. (1)], and $r$ [Eq. (28)] are obtained graphically four our samples and given in Table I, together with those of Dheer[11] for iron whiskers. $R_0$ refers to the low-field limit for the alloys, to the high-field limit for pure metals. $R_s$ always refers to the low-field limit,



KOHLER PLOT FOR HALL
RESISTIVITY OF IRON

—+— 4-BAND MODEL WITHOUT
      ASYMMETRIC SCATTERING

×   SAMPLE I (Fe)

——  SAMPLE 7 OF DHEER (Fe)
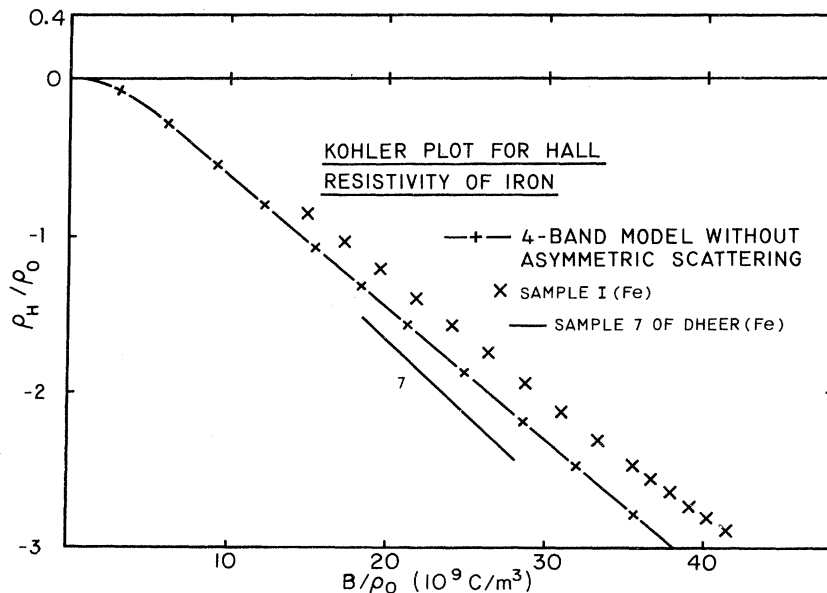
FIG. 7. Theoretical Kohler plot for the Hall resistivity $\rho_H$ of a compensated metal with four bands of different mobilities, without asymmetric scattering. Also shown are the data for two pure-iron samples.
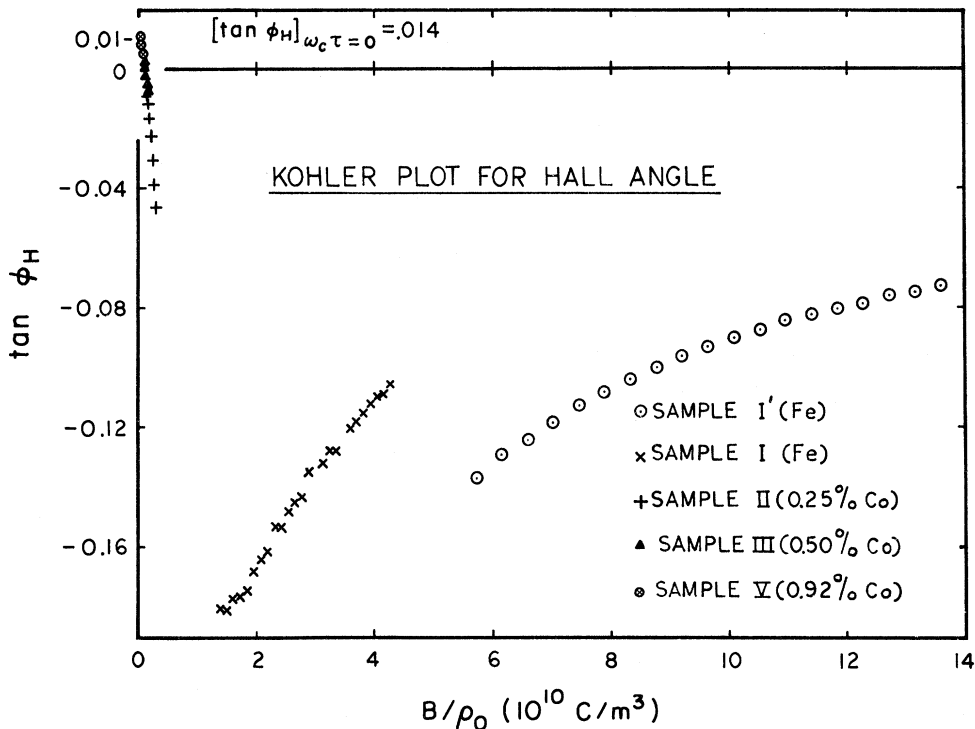
FIG. 8. Kohler plot for the tangent of the Hall angle $\rho_H$ of pure iron and Fe-Co dilute alloys at 4.2 K.

and $r$ to some intermediate-field range. The temperature is 4.2 K unless mentioned otherwise. The resistivity values in zero external field and in zero internal field (or an approximation of it), and the resistivity ratio $\rho_{300}/\rho_0$ are also included.

We note from Table I that, for Fe-Co dilute alloys, the low-field $R_0$ is roughly (within 20%) in-

dependent of impurity concentration, and $R_s$ is approximately proportional to the zero-field resistivity, in agreement with Eqs. (5) and (8), respectively. From the values of $R_0$ and Eq. (7), and from the value $n_e = 2.65 \times 10^{28}$ electrons/m$^3$ derived by us from a rough analysis of existing de Haas–van Alphen periods and band-structure calculations
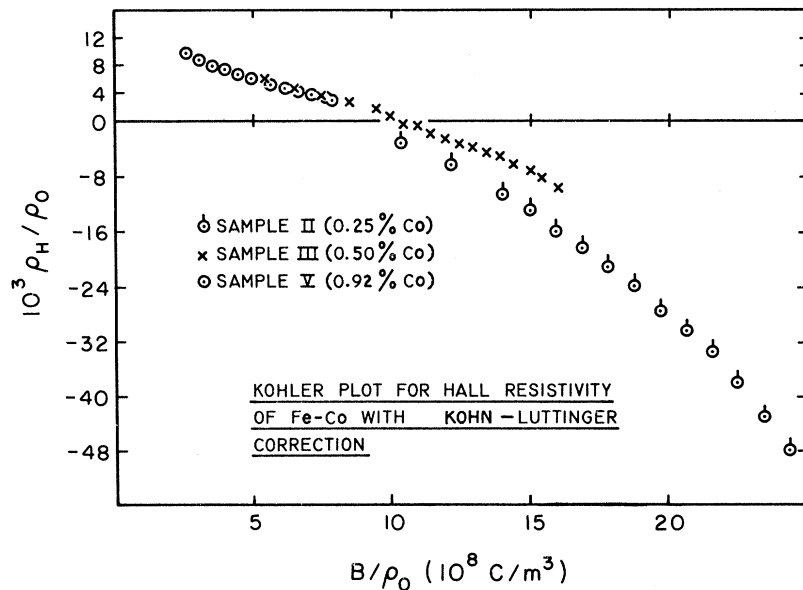
FIG. 9. Kohler plot for the Hall resistivity $\rho_H$ of Fe-Co dilute alloys at 4.2 K on an enlarged scale, with field-independent Kohn–Luttinger correction.

for iron,[41] we get $b \simeq 0.89$ for Fe-Co sample V (low field) and $\simeq 0.32$ for pure-iron sample I' (high field). Thus the electrons are more conducting than holes in pure iron at 4.2 K, while the conductivities are not too different for the Fe-Co alloys.

## IX. FAILURE OF THE LIFSHITZ-AZBEL KAGANOV HIGH-FIELD THEORY IN IRON AND LEAD

In order to study in more detail the Hall angle of pure iron at high fields, we plot in Fig. 10 $\tan\phi_H = \rho_H/\rho$ vs $\rho_0/B$ for the samples I and I' using different horizontal scales. This we call an "inverse" Kohler plot. The solid lines are the best-fitted curves obtained by fitting the data to the two-band model with asymmetric scattering developed in Sec. II.

In the first fitting procedure (Fig. 10), we use $n_e (=n_h)$ as an adjustable parameter. The other parameters are $S_{xx}^e$, $S_{xx}^h$, $S_{xy}^e$ and $S_{xy}^h$. A function-minimization program using the Fletcher and Powell method is used to minimize the least-squares function with respect to the parameters. From the best-fitted parameters the asymptotic value of $\tan\phi_H$ is calculated by Eq. (9), and also the best-fitted curve extending to $\rho_0/B = 0$. One run is shown for each sample.

In another fitting procedure, the fixed value $n_e = n_h = 2.65 \times 10^{28}$ electrons/m$^3$, mentioned above, is assumed.

The experimental data for the sample I' are almost on a straight line. The intercept (point $B$) gives the asymptotic value of $\tan\phi_H = -2.5 \times 10^{-2}$ for this particular run and procedure (Fig. 10). The asymptotic value of $\tan\phi_H$ for sample I' averaged over different runs and the two methods of extrapolation is $(-2.2 \pm 0.5) \times 10^{-2}$. The value for the less-pure sample I (point $A$) is $-2.7 \times 10^{-2}$. However, the extrapolation here is longer, the asymptotic value is less accurate, and the agreement is rather fortuitous. Also, we know that iron has more than two bands[41] and so the fitting is only approximate. Since the impurity nature is difficult to control in pure materials, the high-field Hall angle $\phi_H$ might differ in various samples.

Anyway, we are able to show that there exists a nonzero asymptotic value of $\tan\phi_H$ for iron in the high-field limit, in agreement with Eq. (9). Also, the magnitude of the high-field $\tan\phi_H$ is, within a factor of 2, equal and opposite to the low-field $\tan\phi_H$ of dilute Fe-Co, as predicted by the simplest two-band model with $-S_{xx}^e = S_{xx}^h$.

A similar investigation was done on our lead sample. Like iron, lead is a compensated metal with some open orbits, as found by Alekseevskii and Gaidukov[42] from a study of the galvanomagnetic properties of single crystals.

Extrapolating our transverse magnetoresistance data below the superconducting critical field
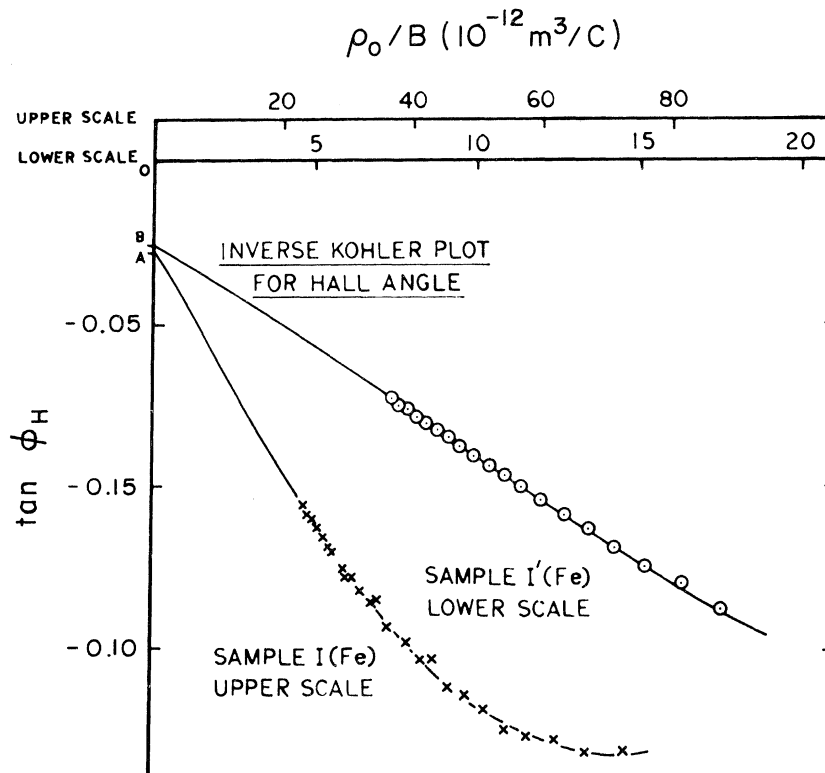


FIG. 10. "Inverse" Kohler plot for the Hall angle $\phi_H$ of pure iron at 4.2 K. Extrapolation to $B/\rho_0 = \infty$ is done by fitting the data to a two-band model with asymmetric scattering. At point $A$, $\tan\phi_H = -0.027$. At point $B$, $\tan \phi_H = -0.025$.
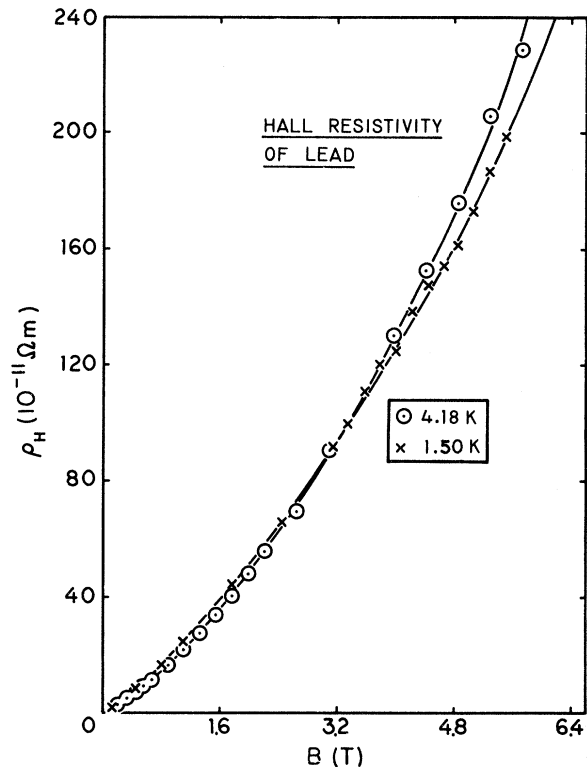
FIG. 11. Hall resistivity $\rho_H$ of pure lead against magnetic field at 4.18 and 1.5 K.

$H_c \approx 0.08$ T gives the zero-field resistivity $= 20 \times 10^{-12}$ $\Omega$ m at 4.18 K (resistivity ratio $= 10\,000$), and $8.2 \times 10^{-12}$ $\Omega$ m at 1.5 K (resistivity ratio $= 24\,300$). The resistivities at 1.5 and 1.96 K differ from each other by at most 3%. This shows

that we are definitely in the residual resistance range at 1.5 K.

A double logarithmic plot of the transverse magnetoresistivity vs $B$ gives $\Delta\rho = \rho - \rho_0 \propto B^{1.81}$ at 4.18 K and $\propto B^{1.84}$ at 1.5 K. For both pure-iron samples we found $\Delta\rho \propto B^{1.86}$ at 4.2 K. These facts imply that the number of grains which are affected by open orbits is rather small for both lead and iron.

The Hall resistivity of lead is plotted in Fig. 11 as a function of field at 4.18 and 1.5 K. Our data show a lot of curvature up to the highest field for both temperatures. The value of $R_0$ at 0.4 T and 4.18 K from our data ($17 \times 10^{-11}$ m$^3$/C) agrees well with those of Borovik[43] ($16 \times 10^{-11}$ m$^3$/C) and Taylor et al.[44] ($15 \times 10^{-11}$ m$^3$/C). Borovik also noticed that $R_0$ depends on the field.

To find the asymptotic value of $\tan\phi_H$ in the high-field limit, $\tan\phi_H$ is plotted vs $1/B$ at 4.18 and 1.5 K in Fig. 12, where we have used different scales for the two temperatures. A graphical extrapolation to $B = \infty$ gives a finite value $\tan\phi_H \simeq 0.06$ at 4.18 K and $\simeq 0.02$ at 1.5 K.

One possible explanation of the nonzero asymptotic $\tan\phi_H$ and of the curvature of the $\rho_H$ data of lead is the following: The impurities present in the lead sample are Si, Cu, Mg, and Fe, each about 1 ppm. The iron impurities, if magnetized by the comparatively large external field, might give rise to asymmetric scattering which in the high-field limit gives $\rho_H \propto M_g B_g^2/c$ and a finite asymptotic $\tan\phi_H$ [see Eqs. (11) and (9)]. However, the magnetization in this case is somewhat field dependent. Collings and Hedgcock[45] showed from susceptibility and ESR experiments that it
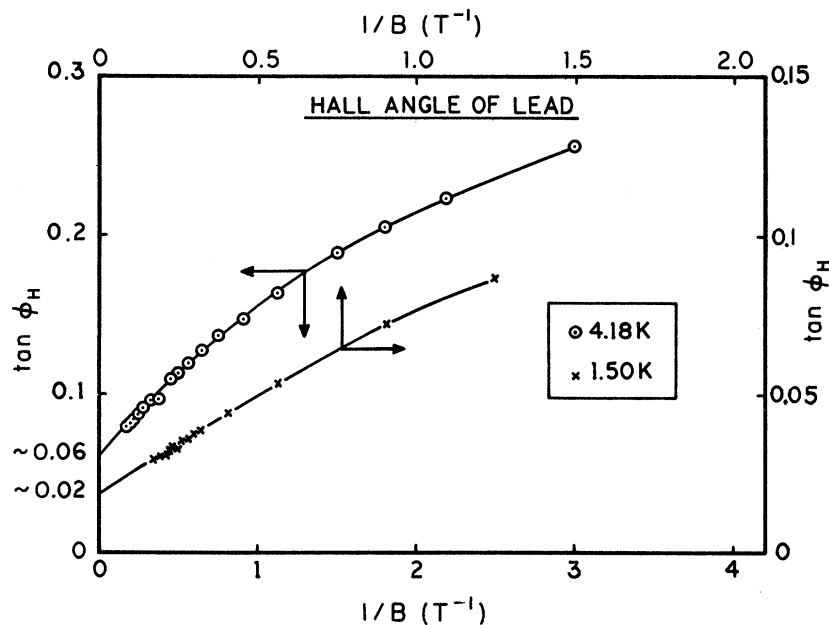
FIG. 12. Hall angle $\phi_H$ of pure lead plotted vs $1/B$ at 4.18 and 1.5 K. Extrapolation to $B = \infty$ is done graphically.

is possible to magnetize iron in magnesium and aluminum, although we do not know of any such measurements with lead as a matrix.

It is not clear why the presence of phonons at 4.18 K should lead to a $\tan\phi_H$ value larger than at 1.5 K.

Asymmetric scattering by paramagnetic impurities such as Fe in a Au matrix, etc., has already been observed[7] in the low-field limit, with $\tan\phi_H \approx 10^{-2}$, the same order of magnitude we find for the high-field limit in Pb.

The large spin-orbit parameter $\bar{\xi}$ of $s$ conduction electrons in a heavy-metal matrix such as Pb and Au ($\bar{\xi} \approx 1$ eV for Pb[46]) leads to $\bar{\xi}/\Delta E_{mn} \gtrsim 0.1$, where $\Delta E_{mn}$ is an interband energy difference. This is at least as large as the ratio found for $3d$ electrons in a Fe or Ni matrix and may explain why similar $\tan\phi_H$ are found in both classes of materials. An effective spin-orbit Hamiltonian, enhanced by a factor of $\approx 3\times10^4$, is probably present around magnetic impurities in lead just as well as in iron or nickel.

## X. IRON-CHROMIUM ALLOYS

Rough values of $\rho_0$ are obtained by extrapolating the longitudinal magnetoresistance back to $B = 0$ (see Sec. VIII). Better values are obtained by adjusting $\rho_0$ so that Kohler's rule is obeyed (Fig. 13) for the longitudinal magnetoresistance of the three samples. Actually only sample I needs to be adjusted, by 4%. The plot of residual resistance against impurity percentage is a straight line having a slope of $25.8\times10^{-9}$ $\Omega$m/wt% compared to the average slope of $23.3\times10^{-9}$ $\Omega$m/wt%, obtained by Arajs $et$ $al.$[17] and Schwerer and Cuddy.[34] A fairly large intercept shows that there are some un-

wanted impurities which contribute about 20% of the residual resistivity of the most dilute Fe-Cr alloy (i.e., sample 1), and much less of the others.

The Kohler plot for the transverse magnetoresistance is shown in Fig. 14 where Kohler's rule barely holds. One should note here that the magnetoresistance plot is fairly sensitive to the choice of $\rho_0$ even in a Kohler plot (where both $B$ and $\rho$ are divided by $\rho_0$) because the origin of the vertical axis is way down from the graph. The discrepancy between samples 1 and 2 is about 20% of $\Delta\rho/\rho_0$ $=(\rho-\rho_0)/\rho_0$. The sample 1 is affected most by the unwanted impurities.

The Kohler plot for the uncorrected $\rho_H$ (Fig. 15) shows clearly that Kohler's rule does not hold here. If we use the same value of $A$ as we did for Fe-Co alloys in Sec. VIII, the Kohn–Luttinger corrections in $\rho_H/\rho_0$ are approximately $0.1\times10^{-2}$, $0.2\times10^{-2}$, and $0.3\times10^{-2}$ for the alloys 1, 2, and 3, respectively. Obviously, applying these small corrections will not make the Kohler's rule work. It should be mentioned here that the uncorrected extrapolated value $\rho_H/\rho_0$ of $\tan\phi_H$ for sample 3 in the low-field limit, obtained from Fig. 15, is $\simeq 0.032$. The magnitude is quite large compared to the corresponding magnitudes of 0.014 (our Fe-Co), 0.011, 0.011, and 0.022 (Huguenin and Rivier's[6] Ni-Fe, Ni-Co, and Ni-Cu, respectively). The reproducibility ($\simeq 2\%$) of the data is checked by annealing a new piece of sample 1 in dry-$H_2$ atmosphere and repeating all measurements and also by taking at least two runs for each sample. To check whether the phonons have anything to do with the failure of Kohler's rule all measurements have been taken at 1.35 K for sample 2 for the



KOHLER PLOT FOR LONGITUDINAL MAGNETORESISTANCE OF Fe-Cr

Ó SAMPLE 1 (0.25% Cr)
x SAMPLE 2 (0.54% Cr)
⊙ SAMPLE 3 (0.98% Cr)
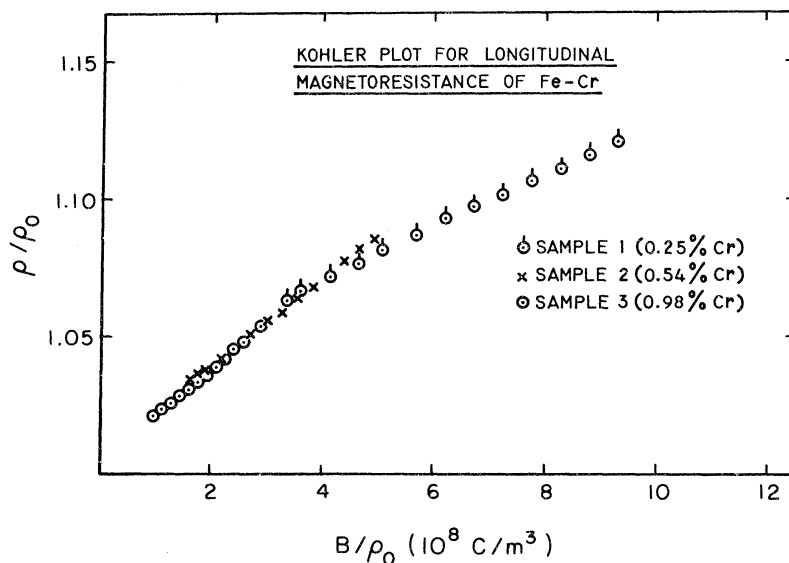
FIG. 13. Kohler plot for the longitudinal magnetoresistance $\rho$ of Fe-Cr dilute alloys at 4.2 K.
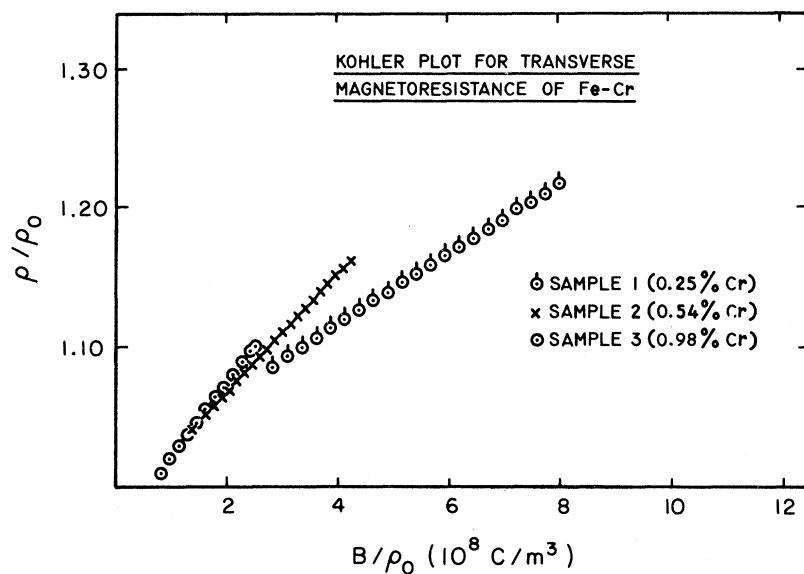
FIG. 14. Kohler plot for the transverse magnetoresistance $\rho$ of Fe-Cr dilute alloys at 4.2 K.

whole range of magnetic fields, and these data agree very well with those at 4.2 K.

Now we propose a few possible ways of interpreting the Hall data in iron-chromium dilute alloys.

*(i)Unwanted impurities.* On the basis of asymmetric scattering theory (Sec. II) and of our data, we are able to show that, in order to explain the discrepancy in terms of asymmetric scattering by the unwanted impurities ( $\simeq 20\%$ of total scattering in our most dilute Fe-Cr alloy), the characteristic low-field asymptotic $\tan\phi_H$ of the unwanted impurities should be larger than $2\times10^{-1}$. This is an order of magnitude larger than any experimental value that we know for iron and nickel dilute

alloys, and is rather unlikely.

*(ii) Impurity overlap.* It may be possible to explain the failure of Kohler's rule for the Hall effect in terms of overlap and interaction of impurity wave functions. Since the residual resistance $\rho_0$ is found to be proportional to the impurity concentration, the overlap, if any, does not seem to affect the residual resistance. Nevertheless, we can not rule out the possibility that it affect the Hall effect.

*(iii)Nonclassical transport.* Combining Eqs. (8) and (23) we obtain (taking $\rho = \rho_0$),

$$R_s = a\rho_0 + A\rho_0^2 \ . \tag{29}$$

If we plot $R_s/\rho_0$ against $\rho_0$ we should get a straight
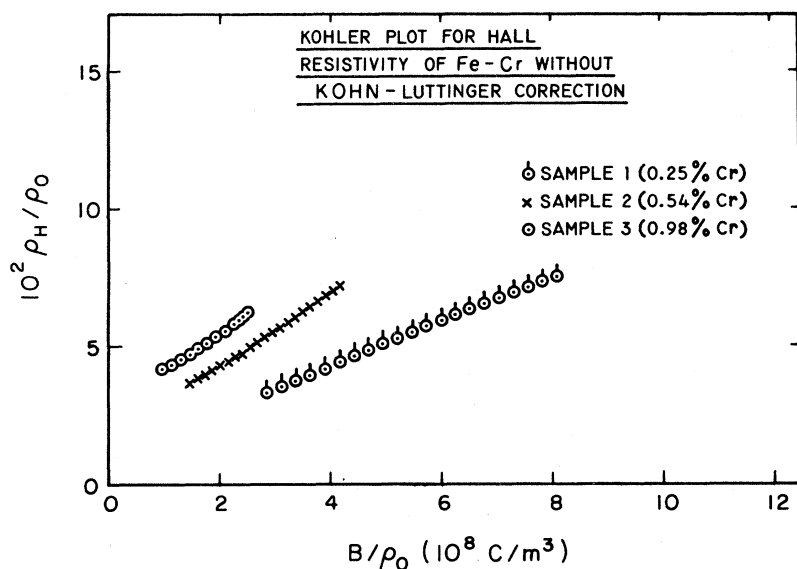


FIG. 15. Kohler plot for the Hall resistivity $\rho_H$ of Fe-Cr dilute alloys at 4.2 K without the Kohn–Luttinger correction.

Fe-Cr ALLOYS          Fe-Co ALLOYS
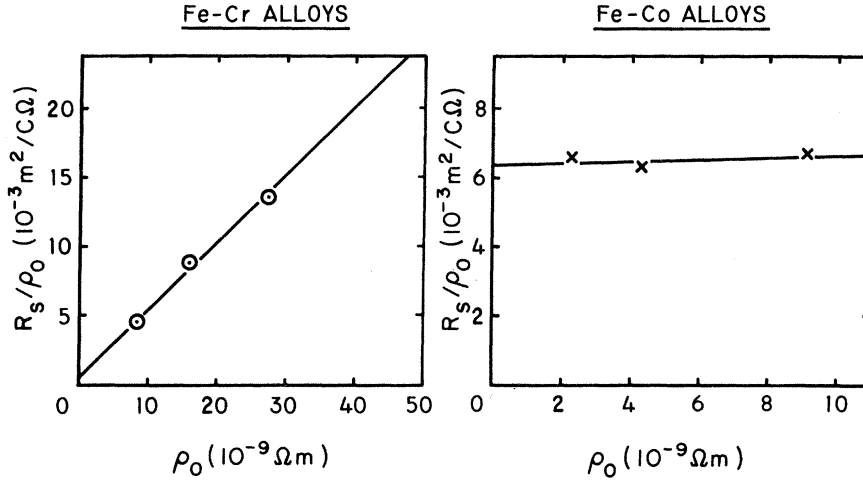


FIG. 16. $R_s/\rho_0$ is plotted vs $\rho_0$ for the Fe-Cr and Fe-Co dilute alloys, where $R_s$ is the extraordinary Hall constant and $\rho_0$ is the residual resistance at 4.2 K.

line with a slope $A$ (Kohn–Luttinger or side jump) and an intercept $a$ (asymmetric scattering). Figure 16 shows such a plot for Fe-Cr and Fe-Co alloys. $R_s$ is obtained from the uncorrected Hall data of Table I. While asymmetric scattering dominates over nonclassical transport in the dilute Fe-Co, the contrary is true in the Fe-Cr. We find $a \approx 0$, $A = 5 \times 10^5$ m/$\Omega^2$C for Fe-Cr.

It is rather puzzling that this value of $A$ is about eight times as large as that given by high-temperature data for iron and many dilute iron alloys (Sec. IV). This large $A$ value implies a large side jump $\Delta y$, by Eq. (24). Instead of the usual $\Delta y \approx 0.1$ nm, one may have $\Delta y \approx 0.8$ nm. This might be related to the large range ($\approx 1.8$ nm) of the zero-point spin disturbance around Cr, as mentioned in Sec. V. However, Lyo and Holstein[3] have shown that $\Delta y$ is completely independent of the potential range, if the $3 \times 10^4$ enhancement factor is itself assumed independent of range. Therefore, one would have to assume here that the enhancement factor is larger for long-range potentials, in order to explain our Cr results. Alternatively, the large $\Delta y$ value might indicate the inadequacy of Born approximation[3(a)] in the presence of the Cr electron scattering resonance.

Only because of that giant side jump is it possible for the nonclassical transport to dominate over asymmetric scattering in a dilute alloy. If it does, Kohler's rule is expected to fail for $\rho_H$ (Fig. 15) and to be replaced by Eq. (26). If the side jump and $\rho_0$ are large enough, one can even neglect normal Hall-effect term in Eq. (26):

$$\rho_H/\rho_0 = M_z \rho_0 f_1(B_z/\rho_0) \qquad (30)$$

In Fig. 17, we show a plot of Eq. (30) in arbitrary units, the even function $f_1$ being taken from the two-band model[3(a)] of side-jump theory for a compensated metal, assuming arbitrarily $T^e_{xx} = -T^h_{xx}$, $T^e_{xy} = -T^h_{xy}$ for simplicity. The values of

$\rho_0$ are chosen in the same ratio as our experimental values for the three Fe-Cr alloys. The experimental range of fields is indicated by a solid line for each curve. Comparing Figs. 15 and 17, we observe that the curves of the various samples are arranged in the same pattern in the theoretical and experimental graphs. The negative intercepts in Fig. 17 (not present in Fig. 15) could easily be removed by a more judicious choice of parameter values. Note that the relatively large slopes in Figs. 15 and 17 should not be described by an ordinary Hall coefficient $R_0$ in terms of the Lorentz force alone as done in Table I. They correspond to an interplay of the Lorentz force and of the side-jump effect [Eq. (30)]. If we were to use Eq. (7), Table I, and $n_e = n_h = 2.65 \times 10^{28}$ electrons/m$^3$ as before, we would obtain $b = 4.7$ for the most concentrated Fe-Cr. But this mobility ratio probably would be spurious.

In Table I, we give also the results of Carter and Pugh[47] for a 0.7-wt%-Cr sample at 4.2 K. They do not agree well with ours.

## XI. RESONANCES AND ASYMMETRIC SCATTERING IN Fe-Cr AND Fe-Co

From Fig. 16 and Eq. (29), we concluded that the asymmetric scattering coefficient $a$ was vanishingly small in Fe-Cr. This implies that the resonance present in $S_{xx}$ or the resistivity of Fe-Cr (Sec. III) is not present in the asymmetric scattering $\tan\phi_H = aM_s$. This is rather in agreement with Sec. III, which predicts a shift between the two resonances. We may be on the dotted line close to point $C$ in Fig. 1.

Since the Cr nuclear charge is smaller than the Fe nuclear charge, the Cr impurity creates a virtually bound state at the top of the $3d$ band. The energy scale of the free-electron model of Sec. III has to be set upside down to apply to that situation. The iron majority-spin carriers have their

THEORETICAL KOHLER CURVE
FOR SIDE-JUMP MODEL

SAMPLE 3

SAMPLE 2

SAMPLE 1
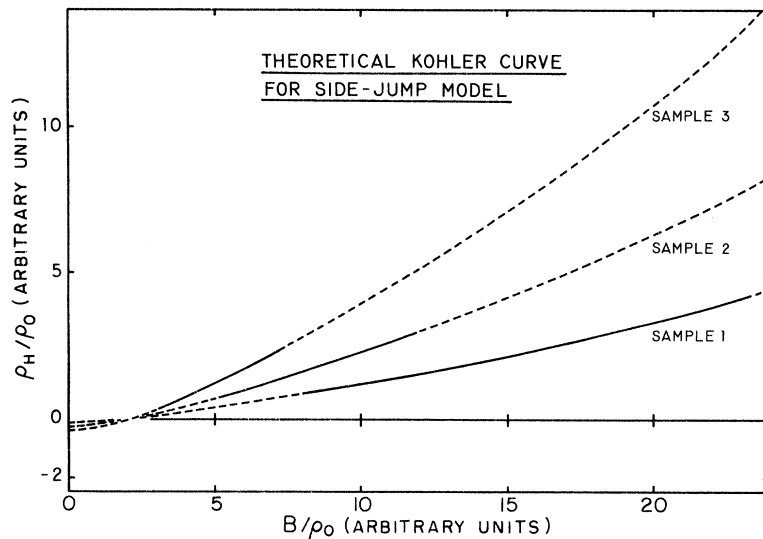
FIG. 17. Rough theoretical Kohler plot for the side-jump model in arbitrary units. The solid lines indicate the experimental range in $B/\rho_0$ for the Fe-Cr dilute alloys.

Fermi level close to the top of the $3d$ band, and sense the virtually bound state as a scattering resonance.

The fact that no scattering resonance is detected with Co, Ni solutes[17] at 4.2 K in Fe is also consistent with the idea of the majority-spin band dominating the conduction, since any virtually bound state on Co, Ni, etc., would be close to band bottom. Such solutes correspond to the right side of Fig. 1.

Note that only the relative sign and magnitude of $\tan\phi_H$ for Fe-Cr and Fe-Co can be compared,

since the absolute sign of the $\approx 10^4$ spin-orbit enhancement factor cannot be predicted.

[*]Work supported by the Army Research Office, Durham and the National Science Foundation.

[†]Present address: Physics Department, Indian Institute of Technology, Kanpur-16, U. P., India.

[1]J.-P. Jan, in *Solid State Physics*, edited by F. Seitz and D. Turnbull (Academic, New York, 1957), Vol. 5, p. 1.

[2]J. Smit, Physica (Utr.) 24, 39 (1958).

[3](a) L. Berger, Phys. Rev. B 2, 4559 (1970); Phys. Rev. B 5, 1862 (1972); (b) S. K. Lyo and T. Holstein Phys. Rev. Lett. 29, 423 (1972).

[4]G. V. Chester and A. Thellung, Proc. Phys. Soc. Lond. 73, 745 (1959).

[5]J. M. Luttinger, Phys. Rev. 112, 739 (1958); W. Kohn and J. M. Luttinger, Phys. Rev. 108, 590 (1957).

[6]R. Huguenin and D. Rivier, Helv. Phys. Acta 36, 808 (1963); Helv. Phys. Acta 38, 900 (1966).

[7]A. Fert and O. Jaoul, Phys. Rev. Lett. 28, 303 (1972).

[8]L. Berger, Phys. Rev. 177, 790 (1969).

[9]J. M. Ziman, *Electrons and Phonons* (Oxford U. P., London, 1960), p. 491.

[10]N. V. Volkenshtein and G. V. Fedorov, Zh. Eksp. Teor. Fiz. 38, 64 (1960) [Sov. Phys.-JETP 11, 48 (1960)].

[11]P. N. Dheer, Phys. Rev. 156, 637 (1967).

[12]W. A. Reed and E. Fawcett, Phys. Rev. 136, A422 (1964).

[13]E. Fawcett, Adv. Phys. 13, 139 (1964).

[14]R. C. Fivaz, Phys. Rev. 183, 586 (1969).

[15]C. W. Chen, Phys. Lett. 7, 16 (1963).

[16]J. Friedel, Nuovo Cimento Suppl. 7, 287 (1958).

[17]S. Arajs, F. C. Schwerer, and R. M. Fisher, Phys. Status Solidi 33, 731 (1969).

[18]W. Jellinghaus and M. P. de Andrés, Ann. Phys. (Paris) 7, 189 (1961).

[19]C. Kooi, Phys. Rev. 95, 843 (1954).

[20]J. P. Jan, Helv. Phys. Acta 25, 677 (1952).

[21]J. P. Jan and H. M. Gijsman, Physica (Utr.) 18, 339 (1952).

[22]G. G. Low, J. Appl. Phys. 39, 1174 (1968).

[23]M. F. Collins and G. G. Low, Proc. Phys. Soc. Lond. 86, 535 (1965).

[24]Yu. A. Izyumov and M. V. Medvedev, Zh. Eksp. Teor. Fiz. 51, 517 (1966) [Sov. Phys.-JETP 24, 347 (1967)].

[25]N. Kroó, L. Pal, M. Aric, and D. Jovic, Phys. Lett. A 28, 213 (1968); N. Kroó, L. Pal, and D. Jovic, in *Neutron Inelastic Scattering* (International Atomic Energy Agency, Vienna, 1968), Vol. II.

[26]G. Delaney, R. E. Thawley, J. Borowska, B. K. Das, and L. Berger (unpublished).

[27]A. U. Seybolt and J. E. Burke, *Procedures in Experimental Metallurgy* (Wiley, New York, 1953).

[28]B. F. Oliver and F. Garofalo, Trans. Met. Soc. AIME 233, 1318 (1965).

[29]R. Morrison, *Grounding and Shielding Techniques in Instrumentation* (Wiley, New York, 1967).

[30]L. Berger and A. R. de Vroomen, J. Appl. Phys. 36, 2777 (1965).

[31]A. I. Schindler and B. C. La Roy, J. Appl. Phys. 37, 3610 (1966).

[32]S. Arajs, B. F. Oliver, and J. T. Michalak, J. Appl. Phys. 38, 1676 (1967).

[33]F. C. Schwerer and J. Silcox, Phys. Rev. B 1, 2391 (1970).

[34]F. C. Schwerer and L. J. Cuddy, Phys. Rev. B 2, 1575 (1970).

[35]R. C. Fivaz, J. Appl. Phys. 39, 1278 (1968).

[36]See, for example, Fig. 4 of J. Yahia and J. A. Marcus [Phys. Rev. 113, 137 (1959)] for gallium.

[37]A. K. Majumdar and L. Berger, J. Appl. Phys. 41, 1423 (1970).

[38]A. C. Ehrlich, R. Huguenin, and D. River, J. Phys. Chem. Solids 28, 253 (1967).

[39]H. Wagenblast and S. Arajs, Phys. Status Solidi 26, 409 (1968).

[40]H. Wagenblast and S. Arajs, J. Appl. Phys. 39, 5885 (1968).

[41]A. V. Gold, in Proceedings of the International Conference on Magnetism, Nottingham, 1964 (The Institute of Physics and the Physical Society, London, 1965), p. 124; J. Appl. Phys. 39, 768 (1968).

[42]N. E. Alekseevskii and Yu. P. Gaidukov, Zh. Eksp. Teor. Fiz. 41, 354 (1961) [Sov. Phys.-JETP 14, 256 (1962)].

[43]E. S. Borovik, Zh. Eksp. Teor. Fiz. 27, 355 (1954).

[44]M. T. Taylor, J. R. Merrill, and R. Bowers, Phys. Rev. 129, 2525 (1963).

[45]E. W. Collings and F. T. Hedgcock, Phys. Rev. 126, 1654 (1962).

[46]J. R. Anderson and A. V. Gold, Phys. Rev. 139, A1459 (1965).

[47]G. C. Carter and E. M. Pugh, Phys. Rev. 152, 498 (1966).

---

# Spin-Orientation Diagrams and Magnetic Anisotropy of Rare-Earth–Iron Ternary Cubic Laves Compounds

U. Atzmony and M. P. Dariel

*Nuclear Research Center, Negev, Beer Sheva, Israel*

E. R. Bauminger, D. Lebenbaum, I. Nowik, and S. Ofer

*The Racah Institute of Physics, The Hebrew University, Jerusalem, Israel*

(Received 4 October 1972)

The directions of the easy magnetization in the $Ho_xTb_{1-x}Fe_2$, $Ho_xEr_{1-x}Fe_2$, $Dy_xTb_{1-x}Fe_2$, $Dy_xEr_{1-x}Fe_2$, and $Ho_xTm_{1-x}Fe_2$ systems have been determined, as a function of $x$ and temperature by means of the Mössbauer effect in $^{57}Fe$. If the direction of magnetization of each system is described by a $(x,T)$ spin-orientation diagram, it is found that the $(x,T)$ plane is divided into two or three regions, in each of which the direction of magnetization is along a different major crystal axis. Theoretical calculations based on the assumption that the magnetic crystalline anisotropy is due to the anisotropy of the interaction between the $4f$ electrons of the rare-earth ions with the crystal fields reproduced the general features of the experimental results though small discrepancies remained. Taking into account an additional contribution to the anisotropy attributed to the Fe-Fe interaction improved the agreement between the theoretical and experimental spin-orientation diagrams. From the theoretical fits to the experimental results a value of $(-0.038\pm0.003)a_0^{-2}$ is derived for the ratio of the crystal field parameters $A_6/A_4$. The transitions between the regions of the spin-orientation diagrams are not sharp. Possible reasons for the existence of the transition regions are discussed.

## I. INTRODUCTION

Cubic Laves phases (type $MgCu_2$) are found in most rare-earth–iron binary systems. The magnetic properties of these compounds have been extensively investigated in recent years by neutron-diffraction, magnetic-susceptibility, and Mössbauer-effect measurements. All $RFe_2$ ($R$ is a rare earth) compounds order magnetically and their magnetic ordering temperatures are around 600 K. Mössbauer studies on $^{57}Fe$ have shown that even though these compounds have an identical crystallographic structure, they present several

types of spectra.[1] The appearance of the different spectra was accounted for in terms of the direction of the easy magnetization axis relative to the crystallographic axes of the unit cell in the respective compounds. With the direction of easy magnetization $\vec{n}$ along the [100] axis, all iron atoms are equivalent and a simple six-line spectrum is obtained, as was observed for $HoFe_2$ and $DyFe_2$. If $\vec{n}$ is along the [111] direction, two magnetically inequivalent iron sites with relative population 3 : 1 exist, giving rise to a spectrum which is a superposition of two six-line patterns, as observed for $YFe_2$, $TbFe_2$, $ErFe_2$, and $TmFe_2$. With $\vec{n}$ parallel